RSC Advances

PAPER

Cite this: *RSC Adv.*, 2015, **5**, 37405

CO_2 reforming of CH_4 over Ni/mesostructured silica nanoparticles (Ni/MSN)†

S. M. Sidik,[a] A. A. Jalil,*[ab] S. Triwahyono,[c] T. A. T. Abdullah[ab] and A. Ripin[ab]

Received 11th March 2015
Accepted 20th April 2015

DOI: 10.1039/c5ra04320d

www.rsc.org/advances

The development of supported Ni-based catalysts for CO_2 reforming of CH_4 was studied. Ni supported on mesostructured silica nanoparticles (MSN) and MCM-41 were successfully prepared using an *in situ* electrochemical method. The N_2 physisorption results indicated that the introduction of Ni altered markedly the surface properties of MCM-41 and MSN. The TEM, H_2-TPR and IR adsorbed CO studies suggested that most of the Ni deposited on the interparticles surface of MSN have higher reducibility than Ni plugged in the pores of MCM-41. Ni/MSN showed a higher conversion of CH_4 at about 92.2% compared to 82.6% for Ni/MCM-41 at 750 °C. After 600 min of the reaction, Ni/MCM-41 started to deactivate due to the formation of shell-like carbon which may block the active sites and/or surface of catalyst, as proved by TEM analyses. Contrarily, the activity of Ni/MSN was sustained for 1800 min of the reaction. The high activity of Ni/MSN was resulted from the presence of greater number of easily reducible Ni on the surface. In addition, the large number of medium-basic sites in Ni/MSN was capable to avoid the formation of shell-like carbon that deactivated the catalyst, thus increased the stability performance. The results presented herein provide new perspectives on Ni-based catalysts, particularly in the potential of MSN as the support.

Introduction

CO_2 reforming of CH_4 has advantages over existing industrial processes for synthesis gas production, from both environmental and industrial perspectives. CO_2 reforming of CH_4 not only converts CO_2 and CH_4, which are recognized as undesirable greenhouse gases, into more desirable products, but also offers an alternative route for the production of syngas with a low H_2/CO molar ratio.[1] During recent decades, considerable efforts have been focused on the development of catalysts for CO_2 reforming of CH_4 in order to achieve high catalytic activity with a high resistance to coking. Although some formulations based on noble metals are very stable and active, Ni-based catalysts present the best balance between economic viability and catalytic performance.[2] However, the major obstacle encountered in the industrialization of CO_2 reforming of CH_4 over Ni-based catalysts, is the rapid deactivation of the catalyst, which is mainly caused by coke accumulation on the active sites and sintering of the active metallic phase.[3] Therefore, improvement of the catalyst stability remains an important challenge.

A strategy that can be used to address coke deposition is to enhance the metal dispersion and to increase the number of basic sites. Sintering of metallic Ni particles on conventional supports, such as Al_2O_3 and SiO_2, is inevitable at high reaction temperatures in the CO_2 reforming of CH_4.[4] This is due to the relatively large Ni particle size (more than 10 nm), which is not small enough to achieve high anti-sintering and coke-resistant properties.[5] Recently, we reported a new method for the preparation of metal nanoparticles using a simple electrochemical method and its successful application in the synthesis of various types of drug precursors.[6,7] By applying the corresponding method, Zn- and Ni-promoted zeolite catalysts led to the efficient isomerization of petrochemical products.[8,9]

The incorporation of Ni particles into mesoporous silica supports has been shown to provide a high dispersion of Ni particles, and hence has improved the stability of Ni catalysts in CO_2 reforming of CH_4.[10,11] In recent years, mesoporous silica nanoparticles (MSN) with a highly ordered mesostructure, a high surface area and a large pore volume have been effectively utilized in the fields of adsorption, drug delivery and catalysis.[5,12,13] One of the important features of MSN compared to other mesoporous silica is their interparticles textural porosity that gives rise to surface area and basicity. This material presents an opportunity for the design of highly accessible active sites on the surface of interparticles voids, which contribute to a better reaction between the reactant and catalyst. However, no studies

[a]*Department of Chemical Engineering, Faculty of Chemical Engineering, Universiti Teknologi Malaysia, 81310 UTM Johor Bahru, Johor, Malaysia*

[b]*Institute of Hydrogen Economy, Universiti Teknologi Malaysia, 81310 UTM Johor Bahru, Johor, Malaysia*

[c]*Department of Chemistry, Faculty of Science, Universiti Teknologi Malaysia, 81310 UTM Johor Bahru, Johor, Malaysia*

† Electronic supplementary information (ESI) available. See DOI: 10.1039/c5ra04320d

of CO_2 reforming of CH_4 have been reported to date using MSN catalyst, notwithstanding some reports over mesoporous silica impregnated with Ni catalysts. These features led to an interest in exploring the potential of MSN as a new support material in CO_2 reforming of CH_4.

In this study, a highly dispersed Ni nanoparticles supported on mesostructured silica nanoparticles (Ni/MSN) was synthesized using an electrochemical method. Ni-supported on mesoporous MCM-41 (Ni/MCM-41) was also synthesized using the same technique to be used as part of a comparative study. By means of various characterization techniques, the physicochemical properties of the catalysts were investigated. The catalytic performances for CO_2 reforming of CH_4 were evaluated and compared, and the relationships between catalytic behavior and property of catalysts have been established. In particular, the catalyst deactivation aspect has been discussed in detail.

Experimental

Synthesis of MSN and MCM-41

MSN was prepared by co-condensation and sol–gel method as previously reported.[12] In brief, the cetyltrimethylammonium bromide (CTAB, Merck), ethylene glycol (EG, Merck) and ammonium (NH_4OH, QRec) solution were dissolved in 700 mL of double distilled water with the following mole composition of CTAB : EG : NH_4OH : H_2O = 0.0032 : 0.2 : 0.2 : 0.1. After vigorous stirring for about 30 min at 50 °C, 1.2 mmol tetraethylorthosilicate (TEOS, Merck) and 1 mmol 3-aminopropyl triethoxysilane (APTES, Merck) were added to the clear mixture to give a white suspension solution. This solution was then stirred for another 2 h at 80 °C, and the as-synthesized MSN sample collected by centrifugation at 20 000 rpm. The as-synthesized MSN were dried at 110 °C overnight and calcined at 550 °C for 3 h to remove the impurities. The amino group and surfactant were successfully removed after calcination, as evidenced by the absence of amino and methyl groups in the FTIR results.

MCM-41 was prepared by hydrothermal method based on a report by Iwamoto *et al.* by using dedocyltrimethylammonium bromide $C_{12}H_{25}N(CH_3)_3Br$, colloidal silica and water.[14] This mixture was homogenized at room temperature by stirring. The resulting mixture was loaded into a Teflon bottle in an autoclave and statically heated at 140 °C for 44 h. The product was washed with deionized water and dried at 110 °C overnight. Finally, to remove remaining template ions, the sample was heated in air at a heating rate of 5 °C min^{-1} to 150 °C and then at a rate of 0.2 °C min^{-1} to 600 °C, and held at 600 °C for 6 h.

Introduction of Ni on MSN and MCM-41

In this study, Ni modified MSN (Ni/MSN) was prepared by *in situ* electrochemical method. Platinum (Pt, Nilaco) and nickel (Ni, Nilaco) plates (2 cm × 2 cm) were used as anode and cathode, respectively. Then, 30 mL of *N*,*N*-dimethylformamide (DMF, Merck) solution was added to a one-compartment cell containing tetraethyl ammonium perchloride (TEAP), naphthalene (Fluka) and MSN. Naphthalene was used as a mediator to produce radical anions, which then reduced the Ni cations to give much smaller Ni nanoparticles.[7] The electrolysis was conducted under continuous stirring at a constant current density of 480 mA cm^{-2} and 0 °C under a N_2 atmosphere. The desired Ni content supported on the MSN and the time required for electrolysis was calculated based on the Faraday's law of electrolysis (refer ESI Table S1†), as shown in the following equation,

$$n = \left(\frac{It}{F}\right)\left(\frac{1}{z}\right) \quad (1)$$

where n is the number of moles of Ni, I is the constant current of electrolysis (A), t is the total time the constant current was applied (s), F is Faraday's law constant (96 487 C mol^{-1}), and z is the valence number of ion of the substance (electron transferred per ion).

After electrolysis, the mixture was heated up at 85 °C to remove the remaining solvents before being dried overnight at 110 °C. Finally, the sample was calcined at 550 °C for 3 h to give a grey-colored Ni/MSN catalyst. For comparative study, Ni/MCM-41 was synthesized under identical experimental conditions as described above. Ni/MCM-41 was also prepared by wet impregnation method for comparison study. The aqueous nickel nitrate ($Ni(NO_3)_2 \cdot 6H_2O$) was impregnated on the MCM-41 at 60 °C, and was then dried in an oven at 110 °C overnight before calcination in air at 550 °C for 3 h.

Characterization

The crystalline structure of the catalysts was determined with X-ray diffraction (XRD) recorded on powder diffractometer (Bruker Advance D8, 40 kV, 40 mA) using a Cu Kα radiation source in the range of 2θ = 1.5–80°. N_2 adsorption–desorption isotherms were used to determine the textural properties at liquid nitrogen temperatures using a Micromeritics ASAP 2010 instrument. The Brunauer–Emmett–Teller (BET) and Non Localized Density Functional Theory (NLDFT) methods were used to calculate the surface area and pore distribution of the catalysts, respectively. Prior to measurement, all of the catalysts were outgassed at 110 °C for 3 h before being subjected to N_2 adsorption at −196 °C. The elemental analyses of Ni content in a catalyst were determined with Agilent Technologies 4100 MP-AES. ^{29}Si MAS NMR spectra were obtained on a Bruker Solid NMR (JEOL 400 MHz) spectrometer. The ^{29}Si MAS NMR signal of tetramethylsilane (TMS) was used as the chemical-shift reference. The spectra were recorded using 4 μs radio frequency pulses, a recycle delay of 60 s and spinning rate of 7 kHz using a 4 mm zirconia sample rotor. Fourier Transform Infrared (FTIR) measurements were carried out using Agilent Technologies Cary 640 FTIR Spectrometer. The catalyst was prepared as a self-supported wafer and placed in a high-temperature stainless steel cell with CaF_2 windows. Then, the catalyst was reduced in H_2 stream (15 mL min^{-1}) at 400 °C for desired reduction periods, followed by outgassing at 400 °C for 1 h. The adsorption of pyrrole was carried out at room temperature for 30 min, followed by desorption at 50, 100 and 150 °C for 15 min, respectively. For the CO adsorption process, the reduced catalyst was exposed to 10 Torr of CO for 30 min. All spectra were recorded at room temperature with a spectral resolution of 5 cm^{-1} with five scans. In order to compare

the surface coverage of the adsorbed species between different wafer thicknesses, all spectra were normalized using the overtone and combination vibrations of the lattice between 2100 and 1550 cm^{-1}.[10] H_2-TPR experiments were carried out using Micromeritics Chemisorb 2720 Pulse Chemisorption in 10% H_2/Ar at 10 °C min^{-1}. H_2 chemisorption was measured to investigate the Ni dispersion and Ni surface area of the catalysts. Prior to the chemisorption, 30 mg of the catalyst was reduced with pure H_2 (20 mL min^{-1}) at 900 °C for 1 h. The amount of hydrogen uptake was determined by injecting mixed gas (10% H_2/Ar) periodically into the reduced catalyst. The Ni dispersion and Ni surface area were calculated by assuming that one hydrogen atom occupies one Ni atom. The amount of coke deposits was determined with thermogravimetric-differential thermal analysis (TG-DTA) using a Perkin Elmer TGA7 Thermogravimetric Analyzer. Temperature was programmed from ambient temperature to 900 °C at a heating rate of 10 °C min^{-1} under N_2 flow. Transmission electron microscopy (TEM) was carried out using a JEOL JEM-2100F microscope. The samples were ultrasonically dispersed in acetone and deposited on an amorphous, porous carbon grid.

Catalytic testing

The catalytic CO_2 reforming of CH_4 was conducted in a continuous flow microcatalytic reactor at atmospheric pressure and in a temperature range of 500–800 °C. The gas hourly space velocity (GHSV) was kept constant at 15 000 mL h^{-1} $g_{cat.}^{-1}$. Prior to the catalytic testing, 0.2 g of catalyst was reduced in a H_2 flow of 50 mL min^{-1} for 3 h at 900 °C. The feeding gas flow rate to the reactor was set at 50 mL min^{-1}, with a gas molar ratio of CH_4 : CO_2 : N_2 = 1 : 1 : 1, as N_2 was used as a carrier gas. The effluent gas was analyzed with an online 7820A gas chromatograph (Agilent Technologies) equipped with a Carboxen 1010 column (Sigma-Aldrich) and a thermal conductivity detector (TCD). The CH_4 and CO_2 conversion was reported as percentage of CH_4 and CO_2 converted. The selectivity of the products to H_2, S_{H_2} and CO, S_{CO} were calculated based on the equation describe as follows:

$$S_{H_2} = \frac{[H_2]_{out}}{2([CH_4]_{in} - [CH_4]_{out})} \times 100 \quad (2)$$

$$S_{CO} = \frac{[CO]_{out}}{([CH_4]_{in} - [CH_4]_{out}) + ([CO_2]_{in} - [CO_2]_{out})} \times 100 \quad (3)$$

where $[H_2]_{out}$ and $[CO]_{out}$ are the molar concentration of H_2 and CO produced during the reaction, respectively. Finally, product distribution ratio, H_2/CO was calculated based on eqn (4).

$$\frac{H_2}{CO} = \frac{S_{H_2}}{S_{CO}} \quad (4)$$

Results and discussion

Characterization of the catalysts

XRD is one of the most important techniques for characterizing the structure of ordered materials. Low- and wide-angle XRD patterns of MSN and MCM-41 type catalysts are shown in Fig. 1. Fresh MSN and MCM-41 showed three peaks at 2.35, 4.05, and 4.75° (Fig. 1A), corresponding to the (100), (110), and (200) planes, reflecting the ordered structure of the 2D hexagonal space group (*p6mm*).[15] The introduction of Ni notably decreased the intensity of all peaks and almost eliminated the (110) and (200) peaks of the Ni/MSN, indicating a reduction in the long-range order of the hexagonal arrangement. In addition, the (100) diffraction for Ni/MSN and Ni/MCM-41 shifted to lower angles compared to the fresh MSN and MCM-41 samples, demonstrating an increase in the corresponding unit cell parameters. As shown in Table 1, the unit cell parameters of both MSN and MCM-41 increased with the addition of Ni, from 4.34 and 4.54 nm to 4.46 and 4.61 nm, respectively. The expansion of the unit cell might be due to the substitution of silicon ions (Si^{4+}, ionic radius = 0.41 Å) with the larger Ni ions (Ni^{2+}, ionic radius = 0.69 Å) in the silica framework.[16] In the wide-angle XRD patterns of Ni/MSN (Fig. 1B), two new peaks were observed at 2θ = 43.1 and 62.8° corresponding to the respective (200) and (220) planes of cubic NiO species (JCPDS 78-0643). No NiO crystals were observed on Ni/MCM-41, indicating that the Ni was homogenously dispersed on the support or the crystallite sizes were smaller than the detection limit of XRD.[17] A similar phenomenon was also observed for metal loaded SBA-15 mesoporous and alumina.[15,18]

The N_2 adsorption–desorption isotherms and pore size distributions of the MSN and MCM-41 type are shown in Fig. 2. Both MCM-41 and MSN exhibited type IV isotherm, which is a typical feature for this type of mesoporous material, according to the IUPAC classification.[19] The MCM-41 showed no hysteresis loop, indicating reversible pore filling and emptying. Meanwhile, the MSN exhibited a type H4 hysteresis loop, suggesting a uniform slit shape pores. In spite of having similar isotherm type, there were pronounced differences in their pore structures. A sharp increase in nitrogen uptake was observed in the relative pressure range of 0–0.03 and 0.3–0.4 for MCM-41, showing the presence of both micropores and mesopores. Similarly, the MSN also displayed a clear and sharp adsorption

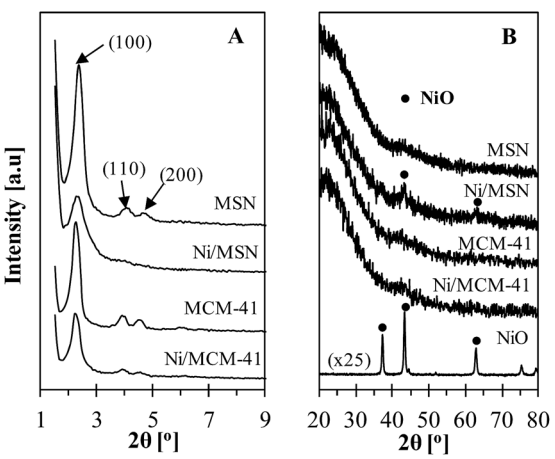

Fig. 1 (A) Low- and (B) wide-angle XRD patterns of MSN and MCM-41 type catalysts.

Table 1 Textural properties of fresh and Ni-modified catalysts

Catalysts	Surface area [m^2 g^{-1}] BET	Micropore[a]	Mesopore[b]	Pore volume [cm^3 g^{-1}]	Pore size[c] [nm]	Unit cell[d] [nm]	Ni dispersion[e] [%]	Ni surface area[e] [m^2 $g_{cat.}^{-1}$]
MSN	894	105	789	0.977	2.58	4.34	n.a	n.a
Ni/MSN	772	25	747	1.001	3.17	4.46	10.5	36.1
MCM-41	877	101	776	0.630	3.78	4.54	n.a	n.a
Ni/MCM-41	337	270	67	0.279	2.70	4.61	11.7	40.2

[a] Micropore area was obtained from *t*-plot method. [b] Mesopore area = Surface area − micropore area. [c] Average pore size was calculated obtained from Non Localized Density Functional Theory (NL-DFT). [d] The unit cell parameter was calculated from unit cell $= 2d_{100}/\sqrt{3}$. [e] Determined from H_2 chemisorption.

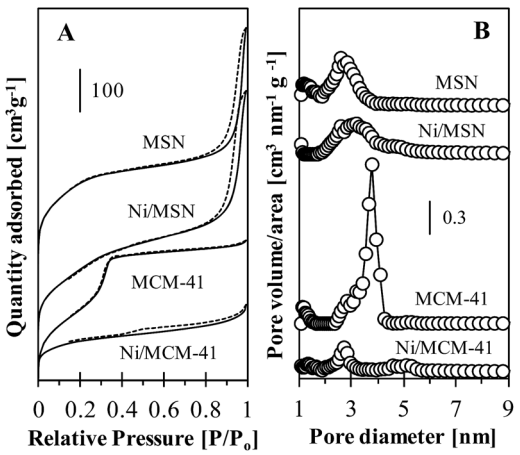

Fig. 2 (A) N_2 adsorption–desorption isotherms and (B) pore size distributions of MSN and MCM-41 type catalysts.

step at a relative pressure in the 0–0.03 range. One of the additional features of MSN is their capillary condensation at higher relative pressure of 0.85–0.95, indicating the presence of larger pores that resulted from interparticles voids. When Ni was incorporated into the MCM-41, the pore filling step at an intermediate relative pressure disappeared. However, the addition of Ni into the MSN decreased the microporosity and slightly increased the interparticles mesopores. Both MSN and MCM-41 showed a narrow pore distribution (Fig. 2B) in the 2–5 nm range. The texture properties of each of the catalysts are summarized in Table 1. The introduction of Ni into MCM-41 significantly decreased the BET and mesopores surface area, and simultaneously increased micropores surface area. Moreover, the average pore size and pore volume of MCM-41 markedly decreased, suggesting the accumulation of Ni particles inside the pore mouth and partially closed the mesopores. Lovell *et al.* reported the formation of smaller NiO can be located in the MCM-41 pores and evidenced by the decrease in pore volume.[20] In contrast, a slight decrease in the BET specific surface area was observed for the Ni/MSN catalyst especially in micropore surface area compared to that of the MSN support. Also, an increase in the pore volume and average pore size was noted, which may be due to the tendency of the Ni species to deposit on the interparticles void of the MSN and blocking the micropores.[21]

The TEM images of Ni/MSN and Ni/MCM-41 are shown in Fig. 3. Some darker gray nanoparticles on the TEM images could be determined as Ni particles. The EDX analysis recorded on the red square area further confirmed that the nanoparticles are Ni. The average particles size of Ni on Ni/MSN is in the range of 3–8 nm, larger than that on Ni/MCM-41 (2–5 nm). From the images, Ni particles were distributed on the interparticles surface of MSN and mostly accumulated at the center of Ni/MCM-41. In accordance to the N_2 physisorption results, it is suggested that most of the Ni nanoparticles filled and/or blocked the pores of MCM-41, whereas most of the Ni nanoparticles were located on the interparticles surface of the MSN.

The FTIR spectra of MSN and MCM-41 type catalysts in the region between 1400 and 400 cm^{-1}, are illustrated in Fig. 4A. For MSN and MCM-41, the bands at 1056 and 797 cm^{-1} were assigned to the asymmetric and symmetric stretching vibrations of Si–O–Si in the framework, respectively. Other bands were observed at 956 and 460 cm^{-1}, corresponded to the external Si–OH groups and Si–O–Si bending, respectively. The addition of Ni shifted the Si–O–Si peaks to lower wavenumbers and simultaneously decreases the external Si–OH and Si–O–Si bending groups. This is suggested that desilication processes occurred and that there was a possible interaction between the Ni species and the Si–O–Si group.[22] The shifts may be attributed to the increase in the mean Si–O distance in the walls of the catalysts, caused by the substitution of silicon with larger Ni atoms.[16] A similar observation was also reported for the substitution of silicon ions in MCM-41 with manganese (Mn^{2+}) and zirconium (Zr^{4+}) ions, which resulted in the shift of the antisymmetric Si–O–Si vibration bands to lower wavenumbers.[22] However, no obvious band was observed in the region of 962–

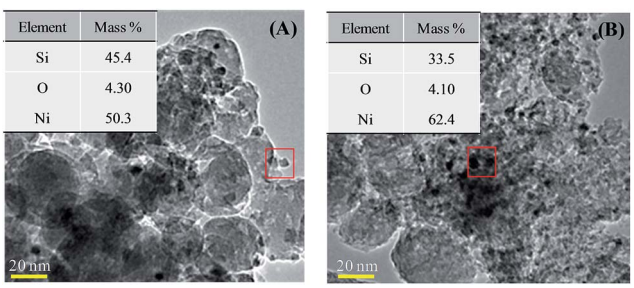

Fig. 3 TEM images and EDX analyses of (A) Ni/MSN and (B) Ni/MCM-41.

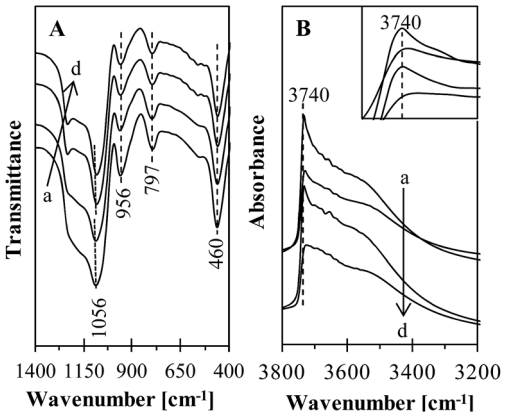

Fig. 4 (A) IR spectra of KBr and (B) activated of (a) MSN, (b) Ni/MSN, (c) MCM-41 and (d) Ni/MCM-41 catalysts.

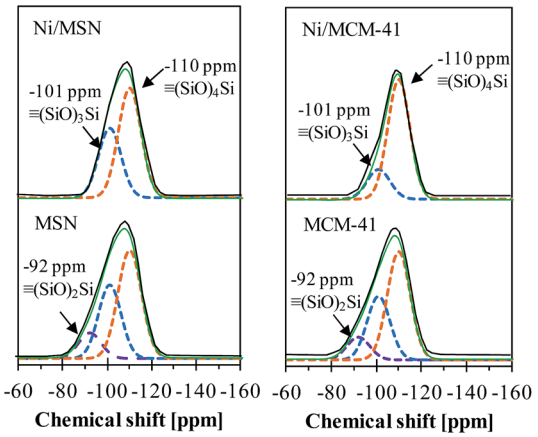

Fig. 5 ^{29}Si MAS NMR spectra of MSN and MCM-41 type catalysts. Green curves represent the Gaussian curve-fitting spectra.

967 cm^{-1}, which corresponds to the vibration of the Si–O–Ni bond. It may be because of an overlap with the characteristic stretching frequencies of siliceous materials in this region.[23]

Fig. 4B shows the FTIR spectra of activated (evacuated at 400 °C for 1 h prior to IR measurement) MSN and MCM-41 type catalysts in the stretching region of the hydroxyl groups at 3200–3800 cm^{-1}. The sharp peak at 3740 cm^{-1} is assigned to the terminal silanol groups located on the external surface of the parent mesoporous.[24] Another broad hydroxyl group on structural defects and/or vicinal hydroxyl groups centered at 3550 cm^{-1} were also observed. The introduction of Ni nanoparticles onto the MSN and MCM-41 decreased the intensity of the terminal silanol, structural defects and vicinal hydroxyl groups, suggesting a possible interaction between the Ni nanoparticles with the Si atom through the O atom. Sapawe *et al.* also found that the decreased in intensity of the hydroxyl groups as the metal loading increased, suggesting increased formation of Si–O–Zr bonds in the catalysts.[25]

^{29}Si MAS NMR spectroscopy offers an excellent opportunity to monitor structural changes and the diversity of silicon environments in the framework of MSN and MCM-41 type catalysts (Fig. 5). The ^{29}Si NMR spectra of MSN and MCM-41 consists of three peaks at −92 ppm, −101 ppm, and −110 ppm, which are attributed to the $(\equiv SiO)_2Si$, $(\equiv SiO)_3Si$, and $(\equiv SiO)_4Si$ structural groups, respectively.[26] The presence of Ni caused a slight decrease in the intensity of the $(\equiv SiO)_4Si$, suggesting the extraction of framework silicon ions from MSN and MCM-41 through the desilication process during the electrolysis process. It is well known that, in alkaline solution, silicon will be selectively removed from its framework. For instance, Qin *et al.* observed a gradual decrease in the intensity of the Si(nAl) peaks with high Si content (n = 0,1) of NaY zeolite after alkali treatment.[27] Similar results were reported by Jusoh *et al.*, who stated that the introduction of ZnO into MSN in an alkaline medium reduced the intensity of the $(\equiv SiO)_4Si$ peak and produced two new peaks for $(\equiv SiO)_3Si$ and $(\equiv SiO)_2Si$.[28] The $(\equiv SiO)_3Si$ peaks were diminished and the $(\equiv SiO)_2Si$ peaks were, infact, featureless for both Ni/MSN and Ni/MCM-41, demonstrating that both free and geminal silanol groups are the active sites for the interaction between the Ni nanoparticles and the supports. These results are in line with FTIR results, which showed interactions between Ni nanoparticles and hydroxyl groups as well as framework silica in the catalysts. In the surface modification of MCM-41 with trimethylchlorosilane, Zhao *et al.* reported a decrease in the intensity of the $(\equiv SiO)_3Si$ and $(\equiv SiO)_2Si$ peaks, suggesting that both sites are responsible for active silylation.[29]

To investigate the reducibility of both Ni/MSN and Ni/MCM-41, H_2-TPR experiments were carried out. The TPR profiles of NiO, Ni/MSN and Ni/MCM-41 were depicted in Fig. 6.

For NiO, there were three reduction peaks at 320, 370 and 391 °C, which can be ascribed to black Ni_2O_3, large and small NiO, respectively.[20] In the case of Ni/MSN and Ni/MCM-41, the reduction peak of Ni_2O_3 shifted to 346 °C, which is due to weak interaction between Ni_2O_3 and MSN. Accordingly, a new broad shouldered peak of hydrogen consumption was observed at 491 °C, which is likely resulted from the reduction of Ni species that strongly interacted with the supports.[30] By comparing the reduction peak at 491 °C, Ni/MCM-41 showed relatively higher hydrogen consumption compared to Ni/MSN, illustrating that the insertion of Ni species most readily deposited in the pore of MCM-41 and resulted in lower reducible Ni species.

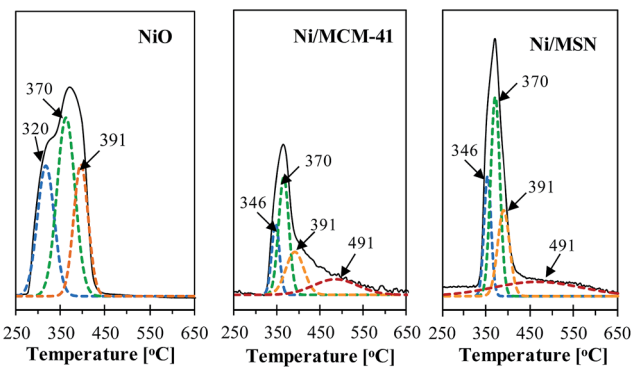

Fig. 6 H_2-TPR profiles of NiO, Ni/MCM-41 and Ni/MSN catalysts.

The metal surface area and metal dispersion for Ni/MSN and Ni/MCM-41 catalysts are compiled in Table 1. From the H_2 chemisorption results, the dispersion of metallic Ni and metal surface area on MCM-41 are higher than those on MSN. The differences are probably due to weaker interaction between Ni and MSN, thus resulting in remarkable nucleation and aggregation of large Ni crystallites during the reduction. On the other hand, the smaller Ni particles that are strongly interacted with the MCM-41 prevent the agglomeration or sintering of the Ni nanoparticles.

Infrared spectroscopy of adsorbed CO was also employed to study interaction between CO and reducible Ni in Ni/MSN and Ni/MCM-41. IR spectra of CO adsorbed on reduced Ni/MSN and Ni/MCM-41 are shown in Fig. 7. The spectra consist of three peaks located at 2156, 2105, and 1859 cm^{-1}, which were assigned to different CO adsorption modes. Two peaks at 2156 and 2105 cm^{-1} were attributed to physically adsorbed CO. The peaks at 1859 cm^{-1} could be assigned to the adsorption of CO on Ni^o bridge sites (Ni_2–CO) of the Ni (111) crystalline plane.[31] After 1 h reduction on Ni/MSN, two new bands appeared at 2063 and 2040 cm^{-1}, which correspond to terminally bonded CO and adsorbed nickel tetracarbonyl [$Ni(CO)_4$], respectively.[32] For Ni/MCM-41, no significant peak associated with the formation of either Ni=CO or $Ni(CO)_4$ was observed. This is probably due to incomplete reduction of Ni nanoparticles present inside the MCM-41 pores that originated from the stabilization of the Ni cations in the silica framework.

To further investigate the degree of reducibility of Ni/MSN and Ni/MCM-41, both catalysts were subjected to different reduction periods before CO adsorption. After reduction for 2 h, a new peak at 2040 cm^{-1} corresponding to Ni=CO, was noticed for Ni/MCM-41. At prolonged reduction periods, an additional peak at 2063 cm^{-1} attributed to the formation of $Ni(CO)_4$ was also observed. Meanwhile for Ni/MSN, a longer reduction did not produce new peak; however, it did intensify the signals.

The difference in reduction period of Ni/MSN and Ni/MCM-41 could be reflected the location of Ni nanoparticles, because Ni located on the interparticles surface has a greater reducibility than Ni in the pore walls. In fact, Lim *et al.* found that the anchoring and partial occlusion of metallic clusters on the pore walls were the main reasons for the stabilization of the catalysts against reduction.[33] The H_2-TPR and IR adsorbed CO indicated that Ni deposited on MSN and MCM-41 at different locations. It is, therefore, suggested that the location of Ni is on the interparticles surface of MSN. In contrast, the larger pore size of MCM-41 allowed the Ni nanoparticles to accumulate inside the pores, for which a longer reduction period is needed in order to reduce the Ni nanoparticles.

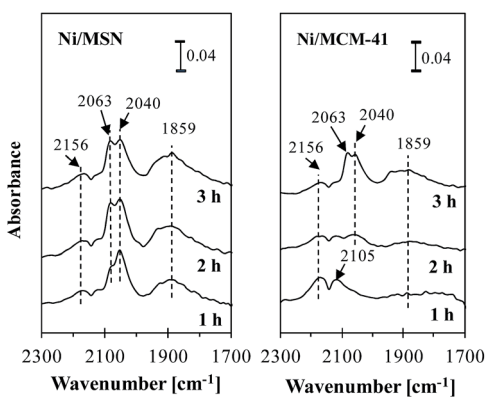

Fig. 7 IR spectra of adsorbed CO on reduced Ni/MSN and Ni/MCM-41 catalysts.

Nature of the basicity

IR spectra of adsorbed pyrrole were obtained for fresh and Ni-modified catalysts to quantitatively measure the strength and the relative amount of basic sites. Fig. 8A shows IR adsorbed pyrrole spectra in which a dotted line indicates the position of N–H from pyrrole molecules in the gas phase which located at 3530 cm^{-1} for all samples. The second band, indicated by an arrow in the figure is attributed to the perturbed N–H stretch of pyrrole molecules interacting with the basic sites of the framework oxygen atoms. The H-donor properties of pyrrole allowed the formation of C_4H_4NH–O bridges with basic oxygen. The asterisk symbol (*) at 3410 cm^{-1} can be assigned to physisorbed pyrrole in a liquid-like state, in which the N–H group is interacting with the π-system of another pyrrole molecule.[34]

The basic sites of the catalyst can be determined based on the area under the main peak. A higher peak area indicates a higher concentration of basic sites in the catalyst. Thus, the number of basic sites in fresh and Ni-modified catalysts increased in the order of MCM-41 < MSN < Ni/MCM-41 < Ni/MSN, as shown in Fig. 8B. The incorporation of Ni nanoparticles into the fresh supports slightly increased the number of basic sites and the basic strength. Previously, Aziz *et al.* have observed a similar basicity in Ni/MSN and Ni/MCM-41 prepared using the impregnation method.[35] This observation may arise from the similar surface area between the catalysts, thus providing an equally accessible site for pyrrole adsorption. In this study, it is worth mentioning that the number of surface

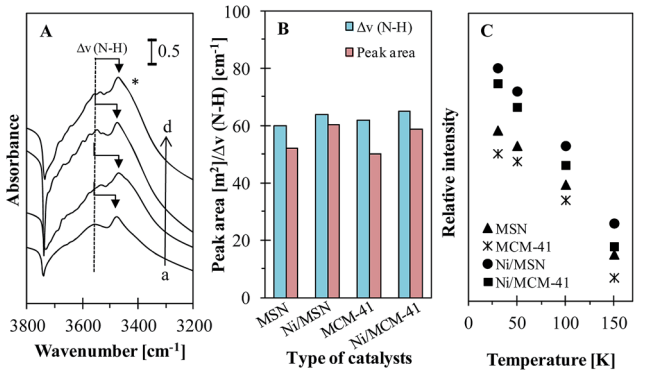

Fig. 8 (A) IR spectra of pyrrole adsorbed on reduced (a) MSN, (b) Ni/MSN, (c) MCM-41 and (d) Ni/MCM-41 when the catalysts were exposed to 4 Torr of pyrrole at room temperature. (B) The shift value of N–H stretching and peak area of basic site of reduced MSN and MCM-41 type catalysts. (C) Effect of desorption temperature on the relative intensity of pyrrole adsorbed on reduced MSN and MCM-41 type catalysts.

basic sites provided by the Ni/MSN is slightly greater than Ni/MCM-41, which may resulted from higher surface area available for pyrrole adsorption.

In addition, the higher intensity of hydroxyl groups in the structural defects in Ni/MSN may contribute to its superior basicity.[36] The IR band associated with N–H vibrations shifted to a lower wavenumber upon the interaction of pyrrole with the basic sites. The strength of the basic sites present in the fresh and Ni-modified catalysts was measured based on the shift of the N–H stretching.[37] As depicted in Fig. 8B, it is suggested that the strength of the basic sites in the fresh and Ni-modified catalysts is in the order of Ni/MCM-41 (-65 cm^{-1}) > Ni/MSN (-64 cm^{-1}) > MCM-41 (-62 cm^{-1}) > MSN (-60 cm^{-1}). Each of these values is slightly lower than the shift observed for the interaction of a H atom in the pyrrole molecule with basic oxygen in an alkali metal supported zeolite ($80 < \Delta\nu$ (N–H) < 150 cm^{-1}). Thus, it is suggested that the pyrrole molecule interacts with catalyst surfaces mainly through the aromatic ring, and the N–H group is assumed to be free or pseudo-free.[38] The strength of the basic sites in the catalyst can also be determined from the effect of the outgassing temperature of the pyrrole adsorbed catalysts. Fig. 8C displays the relative intensity of the main peak of fresh and Ni-modified catalysts at outgassing temperatures between 30 and 150 °C. The intensity of the N–H band interacting with basic sites on the catalysts decreased monotonically with an increase in the outgassing temperature, which can be attributed to the weak interaction between the pyrrole species and the catalysts. Thus, this result suggested that the oxygen in the framework of fresh and Ni-modified catalysts has low electron donor ability, that is, it has medium basicity.

Catalytic testing

The catalytic activity of fresh and Ni-modified catalysts was evaluated according to the degree of conversion of CH_4 and CO_2, the ratio of H_2/CO and TOF of CH_4 conversion at different reaction temperatures. The effect of the reaction temperature on the catalytic performances of Ni/MSN and Ni/MCM-41 is depicted in Fig. 9. Generally, both CH_4 (Fig. 9A) and CO_2 (Fig. 9B) conversions increased with increasing reaction temperature for all catalysts, reflecting the endothermic character of CO_2 reforming of CH_4. The reaction over bare MSN and MCM-41 catalysts showed lower catalytic activity (<5% of CH_4 and CO_2 conversion), indicating that metallic Ni is necessary for the studied catalytic system.

The performances of Ni-modified catalysts were dependent on both the nature of the support materials and the reaction temperature. When the reaction temperature was increased to 600 °C, CH_4 conversion for Ni/MSN reached 54.6% which nearly 1.3 times higher than that of Ni/MCM-41. The conversion of CH_4 increased with the further temperature increase to 800 °C in which the conversion reached 93.6 and 90.8% for Ni/MSN and Ni/MCM-41, respectively. In the range of temperature studied, the activity of Ni/MCM-41 prepared by electrolysis method was slightly higher compared to the Ni/MCM-41 prepared by conventional impregnation method (refer ESI Fig. S1†). At 700 °C, the CH_4 conversion of Ni/MCM-41 is similar

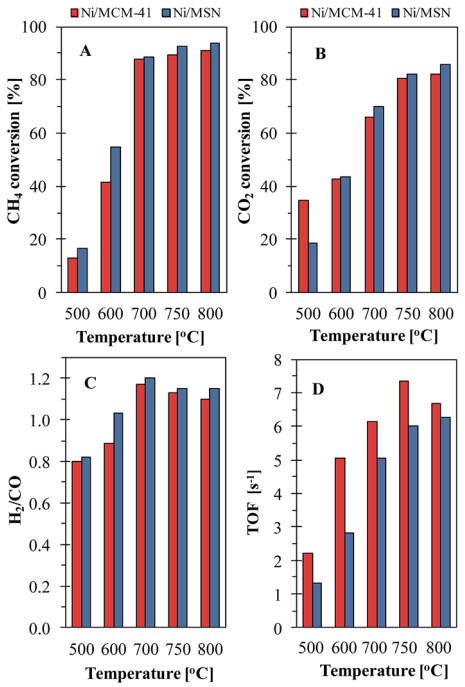

Fig. 9 Effect of reaction temperature on (A) CH_4 conversion, (B) CO_2 conversion, (C) H_2/CO ratio and (D) TOF values over Ni/MSN and Ni/MCM-41 catalysts.

to that reported by Lovell *et al.*[16] for 2.5% Ni/MCM-41 prepared by impregnation method. This finding demonstrates the Ni/MCM-41 and Ni/MSN prepared by *in situ* electrochemical method can produce an activity comparable and greater than MCM-41 prepared by more conventional means, respectively. The activity of Ni/MSN and Ni/MCM-41 catalysts was also compared by turnover frequency (TOF) for CH_4 conversion considering the dispersion of Ni particles as shown in Fig. 9D. The TOF was calculated based on the mole of CH_4 converted per mole of active Ni per second. It is worth noticing that the Ni dispersion and metal surface area of Ni/MCM-41 were larger than those of Ni/MSN due to the formation of smaller Ni particles. On the other hand, the activity of Ni/MSN was found to be 1.2 times higher than Ni/MCM-41 at 750 °C. A significant effect of support is related to the difference of Ni particles size, since a so-called 'structure-sensitive" reaction is influenced by dispersion of metal on the support. Another possibility of support effect may be due to a direct activation of CH_4 or CO_2 by the support. Although no significant activity was observed for fresh MSN, the use of MSN as a support for Ni particles increased the catalytic activity. This indicated a synergistic effect of Ni and MSN on the catalytic activity for CO_2 reforming of CH_4. Although the exact reason is currently unclear, the use of MSN as a support is advantageous for CO_2 reforming of CH_4.

In case of CO_2 conversion, the rate also increased parallel to an increase in the reaction temperature and started to decline at above 750 °C probably due to coking from excess methane dissociation to hydrogen and coke.[39] At 500 °C, CO_2 conversion over Ni/MCM-41 was higher than that of Ni/MSN. From the H_2-TPR analysis, Ni/MCM-41 exhibited lower reducibility than Ni/

MSN. Therefore, reaction at the same feed ratio of CH_4/CO_2 and at low temperature, the Ni sites of Ni/MCM-41 are not capable to adsorbed CH_4 as much as Ni/MSN, which resulted in the increasing of CO_2 adsorption and activation on the Ni/MCM-41 surface. Therefore, a higher CO_2 conversion can be observed for Ni/MCM-41 compared to Ni/MSN.

In this study, Ni/MSN displayed a higher CH_4 and CO_2 conversions than Ni/MCM-41. This is likely to be caused by the presence of more easily reducible Ni nanoparticles on the interparticles surface of the catalyst. This result is in good agreement with a previous study using a Ni/γ-Al_2O_3 catalyst reported by Newnham *et al.*[40] They stated that a higher initial CH_4 conversion was achieved when using the impregnated samples, owing to the presence of Ni particles on the external surface of the catalysts. In addition, some hypotheses suggested that CO_2 is adsorbed at basic sites in the metal–support interface. Thus, the CO_2 conversion could be closely related to the basicity of the catalyst.[41] From the basicity study results shown in Fig. 8, it can be suggested that the number of basic sites is more important compared to the strength of the basic sites. Eventhough Ni/MCM-41 possessed slightly stronger basic sites than Ni/MSN, the greater number of weaker basic sites in the Ni/MSN resulted a higher CO_2 conversion (Fig. 9B).

Fig. 9C shows the relationship of H_2/CO ratio towards the reaction temperature. At 500 °C, the Ni/MSN and Ni/MCM-41 catalysts showed H_2/CO ratios of 0.80 and 0.79, respectively. Although H_2 and CO are formed simultaneously according to the stoichiometry of CO_2 reforming of CH_4, an excess of CO with respect to H_2 was detected. This is probably due to the occurrence of RWGS reactions that consume the produced H_2 and contributed to the production of CO, which would then lower the H_2/CO ratio.[42] As the temperature increased to 600 °C, the H_2/CO ratio was observed to be greater than 1. This indicated that at higher temperatures, the CH_4 cracking reactions were prevalent. This was consistent with previous thermodynamics studies, in which increasing reaction temperatures favored the formation of H_2 through various reactions, such as the Boudouard reaction and CH_4 cracking.[43] The H_2/CO ratio gradually approaches the stoichiometric value of unity as the temperature increases up to 800 °C, implying a balance between the production and consumption of H_2 and CO. It is desirable to obtain a H_2/CO ratio between 0.8 and 2.6, as this is the most appropriate for upstream processing. The H_2/CO ratio (0.80–1.2) produced by the presented CO_2 reforming of CH_4 is, therefore, more appropriate for upstream processing, as a stoichiometric H_2/CO ratio of 3 is obtained from the existing steam reforming process.[20] It is essential to choose 750 °C as the optimal reaction temperature, considering the high catalytic activity and appropriate H_2/CO ratio.

The stability of Ni/MSN and Ni/MCM-41 catalysts for the CO_2 reforming of CH_4 reaction was studied at 750 °C. The results obtained for the CH_4 conversion as a function of time on stream (1800 min), are presented in Fig. 10. The catalytic activity of Ni/MSN remains almost constant throughout the entire 1800 min on stream with a CH_4 conversion of 92.2%. In contrast, the conversion for Ni/MCM-41 started to decline from 89.7 to 85.2% after 600 min time on stream, which may be attributed to the presence of a carbon deposit on the surface of the catalyst. Therefore, a regeneration process was performed at 750 °C with 30 min of air and 1 h of H_2 to remove any deposited carbon from the surface of the catalyst. The catalytic activity of Ni/MCM-41 was recovered after regeneration; however, a slow but apparent deactivation was observed with increasing time on stream after reacting for 720 min. After a second regeneration, the change in the catalytic behavior of Ni/MCM-41 followed the same tendency as it did after the first regeneration, but the values were obviously decreased. The deactivation behavior of Ni/MCM-41 results around 8% of total loss in CH_4 conversion. It is important to note that the stable activity of the Ni/MSN was still observed after a time on stream of 1800 min.

Characterization of spent Ni/MSN and Ni/MCM-41 catalysts

In order to clarify the origin of the deactivation of Ni-modified catalysts, the spent Ni/MSN and Ni/MCM-41 catalysts after 1800 min on stream at 750 °C were characterized by TGA, TEM, and XRD. TGA-DTA analysis was used to estimate the carbon content and species of the spent Ni/MSN and Ni/MCM-41 catalysts, and the results are shown in Fig. 11A. The weight loss was estimated from 110 °C to exclude any interference of moisture. Two exothermic peaks were observed for both spent Ni/MSN and Ni/MCM-4 from the DTG profiles, suggesting that two different types of carbon were deposited. A broad peak centered at 300 °C and 700 °C could be attributed to the oxidation of amorphous carbon and coke deposits with different degrees of graphitization, respectively.[44] A similar amount of carbon (<3%) appeared to be deposited on both the Ni/MSN and Ni/MCM-41.

In order to get insight into the type of carbon on the surface of spent Ni/MSN and Ni/MCM-41, TEM analysis was employed. Fig. 11B shows TEM images of spent Ni/MSN and Ni/MCM-41. Two different types of carbon were formed on spent Ni/MSN and Ni/MCM-41, which consisted of carbon nanotubes and encapsulating carbon (shell-like). Carbon deposit on spent Ni/MSN was mostly in the form of carbon nanotubes with a hollow internal channel, whereas shell-like carbon was mainly formed on spent Ni/MCM-41. It is not surprising that the Ni/MSN catalyst exhibited a very stable catalytic performance in

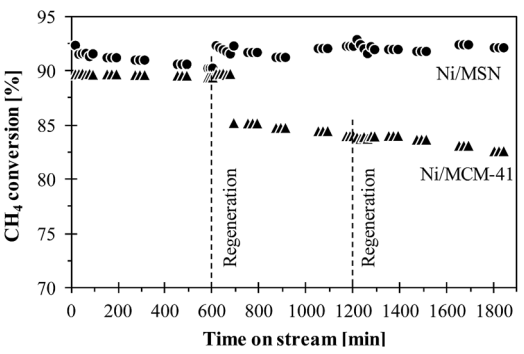

Fig. 10 Stability and regeneration study over Ni/MSN and Ni/MCM-41 catalysts.

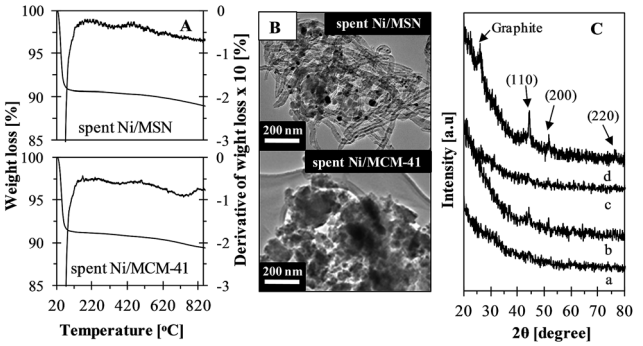

Fig. 11 (A) TG-DTG curves, (B) TEM images and (C) XRD patterns of (a) reduced Ni/MCM-41, (b) spent Ni/MCM-41, (c) reduced Ni/MSN, and (d) spent Ni/MSN catalysts.

the stability evaluation, because the Ni nanoparticles at the tip of carbon nanotubes would still be available and active for CH_4 decomposition. However, the surface coverage of shell-like carbon on Ni/MCM-41 would encapsulate and subsequently reduced the accessibility of the Ni nanoparticles to CH_4 molecules, leading to catalyst deactivation.

The XRD pattern for the reduced and spent Ni/MSN and Ni/MCM-41 catalysts are shown in Fig. 11C. Three new peaks corresponding to metallic Ni were observed at $2\theta = 44.6$, 51.8, and 77.0° for the catalysts, suggesting that all Ni nanoparticles are in the metallic state after the reaction. No evidence could be found for any possible compound formation between Ni and carbon or silica. The Ni/MSN signal exhibited a narrower peak width for the Ni (111) diffraction, which indicates the presence of larger Ni nanoparticles. The average crystallite sizes of the metallic Ni particles calculated using Scherrer equation were increased from 4.2 to 22 nm for Ni/MSN and 2.5 to 17 nm for Ni/MCM-41 after stability test. The smaller Ni crystallite sizes in Ni/MCM-41 may be attributed to the confinement of the Ni nanoparticles in the pores of MCM-41, which prevents the agglomeration or sintering of the Ni nanoparticles. This result suggested that Ni sintering is not the main factor in catalyst deactivation. Moreover, a new peak appeared at $2\theta = 26.1°$ for the spent Ni/MSN, which could be assigned to carbon deposits with a graphitic nature. Recalling that carbon deposits were detected in the TGA for Ni/MCM-41, the absence of graphite diffraction at $2\theta = 26.1°$ indicates that carbon was most probably dispersed on the surface of the Ni nanoparticles inside the MCM-41 pores.

As shown in stability and regeneration study, Ni/MSN showed a stable performance for 1800 min and Ni/MCM-41 showed a partial deactivation after 600 min time on stream. The regeneration of Ni/MCM-41 at 750 °C with air and hydrogen did not recover the catalytic performance and the activity continued to decrease. Characterization of the Ni/MSN and Ni/MCM-41 catalysts after the first regeneration (refer ESI Fig. S2†) indicated that the deactivation of Ni/MCM-41 was likely to be caused by coke accumulation. Eventhough carbon nanotubes were observed on the surface of spent Ni/MSN, the regeneration process successfully removed the deposited carbon. On the other hand, the carbon formed on the surface of Ni/MCM-41 seemed to be more stable and resistant to oxidation, thus continued to deactivate the catalyst. Basically, the carbon species formed both on the support and on the metal can be removed by reaction with adsorbed surface CO_2 and adsorbed oxygen species.[45] The use of supports with a large number of basic sites favors the adsorption and dissociation of CO_2, hence contributes towards the gasification of carbonaceous deposits and prevents deactivation through coke formation.[46] In this study, the ability of Ni/MSN to resist the formation of deactivating carbon deposits compared to Ni/MCM-41 may be related to its basicity. The presence of large number of basic sites resulted from the presence of interparticles voids led to lower coke deposition rates and enhanced the catalyst activity and stability.[47] The carbon nanotubes appeared on the surface of Ni/MSN can be easily remove after regeneration of the catalyst. Therefore, it is suggested that basicity in Ni/MSN is appropriate in attenuating deactivating carbon formation, thus enhancing the stability of the reaction.

Conclusions

Ni supported on MSN and MCM-41 were successfully prepared using an *in situ* electrochemical method. The findings have demonstrated that a higher and more stable catalytic activity could be achieved with Ni loaded on a MSN support than Ni/MCM-41. The characterization results indicated that the different locations of Ni nanoparticles deposited on MSN and MCM-41 could be attributed to the different size of the pores in the supports. H_2-TPR and IR spectra of adsorbed CO indicated that Ni located on the interparticles surface of MSN was more easily reduced and was accountable for the higher CH_4 conversion. Meanwhile, the higher CO_2 conversion on Ni/MSN was caused by the higher basicity, as evidenced from the pyrrole adsorbed IR spectroscopy. In this study, the synergistic effect of Ni location and catalyst basicity was found to be the key factor in the enhanced CO_2 reforming of CH_4 performance over Ni/MSN. The XRD and TEM analyses of the spent catalysts indicated that sintering of Ni nanoparticles did not cause the deactivation, but the stability of the reaction was controlled by the type of carbon deposited on the catalyst. A correlation between basicity and type of coke deposit on the surface of catalyst was observed in the stability evaluation. Ni/MSN showed a stable performance for a time on stream of 1800 min, as a result of the improved basicity, and consequently inhibited the formation of deactivating shell-like carbon. This study showed the potential use of Ni/MSN prepared by electrochemical method in the CO_2 reforming of CH_4.

Acknowledgements

This work is supported by the Universiti Teknologi Malaysia through Research University Grant no. 05H09. Our gratitude also goes to the Ministry of Higher Education (MOHE) Malaysia for the award of MyPhD Scholarship (Siti Munirah Sidik) and the Hitachi Scholarship Foundation for the Gas Chromatograph Instrument Grant.

Notes and references

1 W. Chen, G. Zhao, Q. Xue, L. Chen and Y. Lu, *Appl. Catal., B*, 2013, **136**, 260.
2 D. Baudouin, U. Rodemerck, F. Krumeich, A. Mallmann, K. C. Szeto, H. Ménard, L. Veyre, J.-P. Candy, P. B. Webb, C. Thieuleux and C. Copéret, *J. Catal.*, 2013, **297**, 27.
3 Z. Wang, X.-M. Cao, J. Zhu and P. Hu, *J. Catal.*, 2014, **311**, 469.
4 Ş. Özkara-Aydinoğlu and A. E. Aksoylu, *Catal. Commun.*, 2010, **11**, 1165.
5 Z. Liu, J. Zhou, K. Cao, W. Yang, H. Gao, Y. Wang and H. Li, *Appl. Catal., B*, 2012, **125**, 324.
6 A. A. Jalil, N. Kurono and M. Tokuda, *Synlett*, 2001, **12**, 1944.
7 A. A. Jalil, N. Kurono and M. Tokuda, *Synthesis*, 2002, **18**, 2681.
8 S. Triwahyono, A. A. Jalil, R. R. Mukti, M. Musthofa, N. A. M. Razali and M. A. A. Aziz, *Appl. Catal., A*, 2011, **407**, 91.
9 N. H. N. Kamarudin, A. A. Jalil, S. Triwahyono, R. R. Mukti, M. A. A. Aziz, H. D. Setiabudi, M. N. M. Muhid and H. Hamdan, *Appl. Catal., A*, 2012, **431**, 104.
10 M. A. A. Aziz, A. A. Jalil, S. Triwahyono and M. W. A. Saad, *Chem. Eng. J.*, 2014, **260**, 757.
11 L. Li, S. He, Y. Song, J. Zhao, W. Ji and C.-T. Au, *J. Catal.*, 2012, **288**, 54.
12 A. H. Karim, A. A. Jalil, S. Triwahyono, S. M. Sidik, N. H. N. Kamarudin, R. Jusoh, N. W. C. Jusoh and B. H. Hameed, *J. Colloid Interface Sci.*, 2012, **386**, 307.
13 N. H. N. Kamarudin, A. A. Jalil, S. Triwahyono, N. F. M. Salleh, A. H. Karim, R. R. Mukhti, B. H. Hameed and A. Ahmad, *Microporous Mesoporous Mater.*, 2013, **180**, 235.
14 M. Iwamoto, Y. Tanaka, J. Hirosumi, N. Kita and S. Triwahyono, *Microporous Mesoporous Mater.*, 2001, **48**, 271.
15 N. Wang, W. Chu, T. Zhang and X. S. Zhao, *Int. J. Hydrogen Energy*, 2012, **37**, 19.
16 D. Liu, R. Lau, A. Borgna and Y. Yang, *Appl. Catal., A*, 2009, **358**, 110.
17 U. Izquierdo, V. L. Barrio, K. Bizkarra, A. M. Gutierrez, J. R. Arraibi, L. Gartzia, J. Banuelos, I. Lopez-Arbeloa and J. F. Cambra, *Chem. Eng. J.*, 2014, **238**, 178.
18 L. Xu, Z. Miao, H. Song and L. Chou, *Int. J. Hydrogen Energy*, 2014, **39**, 253.
19 P. Djinović, J. Batista and A. Pintar, *Int. J. Hydrogen Energy*, 2012, **37**, 2699.
20 E. Lovell, Y. Jiang, J. Scott, F. Wang, Y. Suhardja, M. Chen, J. Huang and R. Amal, *Appl. Catal., A*, 2014, **437**, 51.
21 N. Wang, X. Yu, Y. Wang, W. Chu and M. Liu, *Catal. Today*, 2013, **212**, 98.
22 M. Selvaraj, P. K. Sinha, K. Lee, I. Ahn, A. Pandurangan and T. G. Lee, *Microporous Mesoporous Mater.*, 2005, **78**, 139.
23 M. Selvaraj, B. H. Kim and T. G. Lee, *Chem. Lett.*, 2005, **34**, 1290.
24 A. A. Jalil, M. A. H. Satar, S. Triwahyono, H. D. Setiabudi, N. H. N. Kamarudin, N. F. Jaafar, N. Sapawe and R. Ahamad, *J. Electroanal. Chem.*, 2013, **701**, 50.
25 N. Sapawe, A. A. Jalil, S. Triwahyono, S. H. Adam, N. F. Jaafar and M. A. H. Satar, *Appl. Catal., B*, 2012, **125**, 311.
26 X. S. Zhao, G. Q. Lu, A. K. Whittaker, G. J. Millar and H. Y. Zhu, *J. Phys. Chem. B*, 1997, **101**, 6525.
27 Z. Qin, B. Shen, Z. Yu, F. Deng, L. Zhao, S. Zhou, D. Yuan, X. Gao, B. Wang, H. Zhao and H. Liu, *J. Catal.*, 2013, **298**, 102.
28 N. W. C. Jusoh, A. A. Jalil, S. Triwahyono, H. D. Setiabudi, N. Sapawe, M. A. H. Satar, A. H. Karim, N. H. N. Kamarudin, R. Jusoh, N. F. Jaafar, N. Salamun and J. Efendi, *Appl. Catal., A*, 2013, **468**, 276.
29 X. S. Zhao and G. Q. Lu, *J. Phys. Chem. B*, 1998, **102**, 1556.
30 K. Tao, L. Shi, Q. Ma, D. Wang, C. Zeng, C. Kong, M. Wu, L. Chen, S. Zhou, Y. Hu and N. Tsubaki, *Chem. Eng. J.*, 2013, **221**, 25.
31 K. A. Layman and M. E. Bussell, *J. Phys. Chem.*, 2004, **108**, 10930.
32 M. Mihaylov, K. Hadjiivanov and H. Knözinger, *Catal. Lett.*, 2001, **76**, 59.
33 S. Lim, C. Wang, Y. Yang, D. Ciuparu, L. Pfefferle and G. L. Haller, *Catal. Today*, 2007, **123**, 122.
34 J. Kucera and P. Nachtigall, *J. Phys. Chem. B*, 2004, **108**, 16012.
35 M. A. A. Aziz, A. A. Jalil, S. Triwahyono, R. R. Mukhti, Y. H. Taufiq-Yap and M. R. Sazegar, *Appl. Catal., B*, 2014, **147**, 359.
36 L. Xiancai, W. Min, L. Zhihua and H. Fei, *Appl. Catal., A*, 2005, **290**, 81.
37 J. C. Lavalley, *Catal. Today*, 1996, **27**, 377.
38 B. Camarota, Y. Goto, S. Inagaki and B. Onida, *Langmuir*, 2011, **27**, 1181.
39 D. C. Carvalho, H. S. A. de Souza, J. M. Filho, A. C. Oliveira, A. Campos, E. R. C. Milet, F. F. de Sousa, E. P. Hernandez and A. C. Oliveira, *Appl. Catal., A*, 2014, **473**, 132.
40 J. Newnham, K. Mantri, M. H. Amin, J. Tardio and S. K. Bhargava, *Int. J. Hydrogen Energy*, 2012, **37**, 1454.
41 T. Huang, W. Huang, J. Huang and P. Ji, *Fuel Process. Technol.*, 2011, **92**, 1868.
42 J. Z. Luo, Z. L. Yu, C. F. Ng and C. T. Au, *J. Catal.*, 2000, **194**, 198.
43 Y. Li, Y. Wang, X. Zhang and Z. Mi, *Int. J. Hydrogen Energy*, 2008, **33**, 2507.
44 M. Khavarian, S. P. Chai and A. R. Mohamed, *Chem. Eng. J.*, 2014, **257**, 200.
45 D. Pakhare, V. Schwartz, V. Abdelsayed, D. Haynes, D. Shekhawat, J. Poston and J. Spivey, *J. Catal.*, 2014, **316**, 78.
46 J. H. Bitter, K. Seshan and J. A. Lercher, *J. Catal.*, 1997, **171**, 279.
47 Y. H. Guo, C. Xia and B. S. Liu, *Chem. Eng. J.*, 2014, **237**, 421.